Theoretical studies on farnesyltransferase: The distances paradox explained

ARTICLE *in* PROTEINS STRUCTURE FUNCTION AND BIOINFORMATICS · OCTOBER 2006

Impact Factor: 2.63 · DOI: 10.1002/prot.21219 · Source: PubMed

PROTEINS: Structure, Function, and Bioinformatics 66:205–218 (2007)

Theoretical Studies on Farnesyltransferase: The Distances Paradox Explained

Sérgio Filipe Sousa, Pedro Alexandrino Fernandes, and Maria João Ramos*
REQUIMTE, Departamento de Química, Faculdade de Ciências, Universidade do Porto, 4169-007 Porto, Portugal

ABSTRACT **In spite of the enormous interest that has been devoted to its study, the mechanism of the enzyme farnesyltransferase (FTase) remains the subject of several crucial doubts. In this article, we shed a new light in one of the most fundamental dilemmas that characterize the mechanism of this puzzling enzyme commonly referred to as the "distances paradox", which arises from the existence of a large 8-Å distance between the two reactive atoms in the reaction catalyzed by this enzyme: a Zn-bound cysteine sulphur atom from a peptidic substrate and the farnesyldiphosphate (FPP) carbon 1. This distance must be overcome for the reaction to occur. In this study, the two possible alternatives were evaluated by combining molecular mechanics (AMBER) and quantum chemical calculations (B3LYP). Basically, our results have shown that an activation of the Zn-bound cysteine thiolate with subsequent displacement from the zinc coordination sphere towards the FPP carbon 1 is not a realistic hypothesis of overcoming the large distance reported in the crystallographic structures of the ternary complexes between the two reactive atoms, but that a rotation involving the FPP molecule can bring the two atoms closer with moderate energetic cost, coherent with previous experimental data. This conclusion opens the door to an understanding of the chemical step in the farnesylation reaction. Proteins 2007;66:205–218.**

Key words: FTase; mechanisms; carboxylate-shift; DFT; ONIOM; AMBER

INTRODUCTION

Protein farnesyltransferase (FTase), a zinc metalloenzyme, is composed of two nonidentical subunits (α and β) and catalyzes the farnesylation of protein substrates containing a C-terminal CaaX motif, in which C is the cysteine that is farnesylated, "a" is usually an aliphatic amino acid, and X is the terminal amino acid, normally methionine, serine, alanine, or glutamine.[1–5] Farnesyldiphosphate (FPP) is the typical isoprenoid farnesyl donor. Among the known substrates for FTase are H-, N-, and K-Ras proteins, nuclear lamins A and B, the γ subunit of heterotrimeric G-proteins, centromeric proteins, and several proteins involved in visual signal transduction.[6–8]

The discovery that farnesylation is absolutely required for oncogenic forms of Ras proteins to transform cells[9–11] has promoted widespread interest in FTase, given that mutant Ras proteins have been implicated in something like 30% of all human cancers.[12–14] Examples include pancreatic adenocarcinomas (90%), colon adenocarcinomas and adenomas (50%), lung adenocarcinomas (30%), myeloid leukemias (30%), and melanomas (20%).[13,14] Several FTase inhibitors (FTIs) have been undergoing clinical trials for cancer treatment,[15–22] and more than 100 patents describing FTIs have been published since 2000.[23] Possible roles in the treatment of some parasitic infections, such as malaria,[24–29] African sleeping sickness,[30–32] Chagas disease,[33–35] Toxoplasmosis[36] and Leishmaniasis,[33] and as antiviral agents against viruses that require farnesylation by the host FTase in key aspects of their own life cycles[37] have also been postulated. This last aspect can be of particular importance since among these viruses are several potential agents of bioterrorism.[37]

Despite the enormous curiosity surrounding FTase inhibition and the vast research in the field, several fundamental doubts on the farnesylation mechanism still remain.[38] A better comprehension of this mechanism could lead to significant progresses in the development of more specific FTIs, with increased activity for cancer treatment, with potential value in the treatment of parasitic infections, or even with application as antiviral agents. Presently, all the available FTase crystallographic structures for the ternary complex (FTase-FPP-peptide substrate)[39–41] show a distance of more than 7.5 Å between the two reactive atoms (the C1 of FPP and the peptide thiolate sulfur) (Fig. 1). This distance must be reduced for the reaction to occur. Two alternatives are possible. One of the hypothesis suggests that the peptide thiolate dissociates from zinc with simultaneous translocation nearer to FPP.[42–44] The other alternative proposes a movement of the FPP carbon 1 (C1) towards the

Grant sponsor: Fundação para a Ciência e a Tecnologia (FCT); Grant numbers: POCI/QUI/61563/2004, SFRH/BD/12848/2003.

*Correspondence to: Maria João Ramos, REQUIMTE, Departamento de Química, Faculdade de Ciências, Universidade do Porto, Rua do Campo Alegre, 687, 4169-007 Porto, Portugal.
E-mail: mjramos@fc.up.pt

Received 15 March 2006; Revised 1 August 2006; Accepted 10 August 2006

Published online 26 October 2006 in Wiley InterScience (www.interscience.wiley.com). DOI: 10.1002/prot.21219

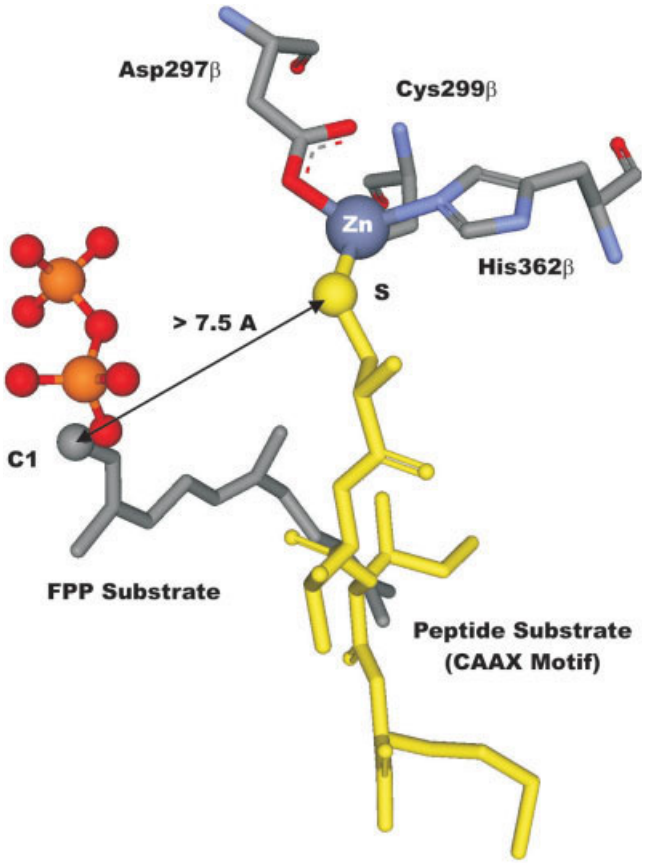

Fig. 1. The "Distances Paradox"—Schematic representation of the active-site Zn coordination sphere, peptide substrate and FPP, illustrating the very large distance reported in all crystallographic structures between the two reactive atoms that must be overcome for the chemical step to occur. [Color figure can be viewed in the online issue, which is available at www.interscience.wiley.com.]

zinc-bound peptide thiolate, through a rotation involving the two first isoprene subunits.[45,46] The dilemma discussed is of the uttermost importance in the farnesylation mechanism and is normally referred to as the "distances paradox."[38] Solving this aspect would enable a better understanding at the atomic level of the reaction catalyzed by FTase.

In this study, both alternatives were investigated using molecular mechanical and quantum chemical calculations, taking into consideration the available X-ray crystallographic structures, extended X-ray absorption fine structure (EXAFS) results,[47] and several kinetic and mutagenesis experiments,[42–44,48,49] together with new important mechanistic facts obtained from recent studies,[45,50–54] and in particular, the proved existence of a carboxylate-shift mechanism.[47,49,53]

METHODOLOGY

FPP Rotation Hypothesis

Context

In this part of the work, the FPP rotation hypothesis was evaluated by approaching the FPP C1 from the Zn coordinate peptide thiolate (SR), considering the full enzyme and employing molecular mechanics (MM). This method was employed as no bond-breaking or bond-forming process and is required to be taken into account to assess the feasibility of this conformational alteration. Furthermore, the dependence of such an alteration on the enzyme structure limits any drastic simplifications on the model size. The process was performed considering both a peptide substrate (CVIM) and a nonsubstrate peptide inhibitor (CVFM) to disclose possible trends in activity and explain the known reactivity patterns.

Calculations

The enzyme structures for the process were prepared from the crystallographic structure with both FPP and a peptide with the best resolution–1JCR (ternary complex FTase-FPP-CVFM, resolution 2.00 Å).[41] The peptide substrate CVIM from the structure 1D8D[40] was later modeled into 1JCR active site at the position of the nonsubstrate peptide inhibitor CVFM. Two systems were therefore produced: the substrate system (FTase-FPP-CVIM) and the inhibitor system (FTase-FPP-CVFM). Conventional protonation states for all amino acids at pH 7 were considered. All the hydrogens were added, and Na^+ ions were placed using the Leap program to neutralize the highly negative charge (−24) of the model systems. The systems were then placed in rectangular boxes containing TIP3P water molecules with a minimum distance of 15.0 Å of water molecules between the enzyme and the box side. The total number of atoms in each system was 133,897 and 133,998, respectively for the substrate and the inhibitor models. Both systems were subjected to a 4-stage refinement protocol in which the constraints on the enzyme were gradually removed. In the first stage (10,000 steps), 50 kcal/mol/Å^2 harmonic forces were used to restrain the positions of all atoms in the systems except the ones from the water molecules. In the second stage (10,000 steps), these constraints were applied only to the heavy atoms, and in the third stage (30,000 steps) were limited to the CA and N atom-type atoms (backbone α carbons and nitrogens). This process ended in a full energy minimization (4th stage, maximum 80,000 steps) until the rms gradient was smaller than 0.02 kcal/mol. The AMBER 8.0[55] molecular dynamics package was used in the entire process, together with new molecular mechanical parameters specifically designed for FTase that have been extensively validated against EXAFS data, a total of seven X-ray crystallographic structures of the FTase ternary complex, and high-level quantum calculations with two types of models of different sizes.[56] All energy minimizations were carried out using the SANDER module of AMBER 8.0 and considering periodic boundary conditions to simulate an infinite system. The particle-mesh Ewald method[57] with a nonbond-interaction cut-off radius of 10 Å was considered.

Two linear transit scans were then performed by gradually approaching the FPP C1 from the Zn-bound pep-

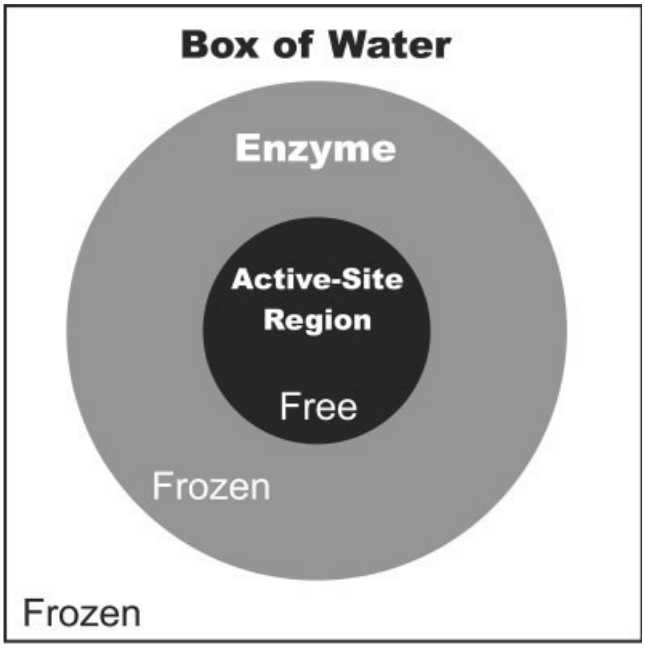

Fig. 2. Approximation considered in the FPP scan performed with the full enzyme placed in a box of waters.

tide thiolate (SR). In this process, constraints were applied to the enzyme and box of waters, with the exception of the FPP molecule, Zn coordination sphere and a selection of residues within a 12 Å radius of these two key active-site elements (Fig. 2). The choice on the size of the free portion of the system was carefully made as to allow, on one hand the effective optimization of the model (both in terms of accuracy and swiftness), and on the other hand induced alterations on the position of neighboring residues. The initial step size (0.2 Å) was also chosen based on the same criteria. With these conditions, a strict 0.0001 kcal/mol convergence criterion was achieved for all intermediate structures. The use of significantly larger free regions (including a fully unfrozen system) were tested in an earlier stage, but rendered major convergence problems and inconsistent energy variation trends due to nonlocal effects. This difficulty in geometry optimizations of large systems has been previously discussed in literature.[58] The huge number of degrees of freedom typically involved in such systems frequently causes local minima to be achieved that differ in the hydrogen-bonding network or with regard to other conformational changes, leading to major energy variations that are completely unrelated to the problem under investigation, and hence absolutely misleading. In fact, in some of the initial tests performed, very large energy differences were commonly observed for consecutive optimized structures where the distance between the two reactive atoms had been changed by only 0.2 Å, and the backbones of the optimized enzyme structures were completely superimposable or diverged on rather small and remote structural features, an effect already pointed out and discussed in literature.[58] It is therefore normally advisable to restrict the optimization process to the minimum acceptable region in order to allow the control over such factors.[58] The alternative approach to the problem in question consisted on employing molecular dynamics simulations to each of the intermediate states. However, such an approach was discarded both due to the huge size of the systems and the long simulation time that would be required to obtain meaningful statistical energies for each of the intermediate geometries. Rather than obtaining or characterizing the real approximation pathway, our aim on tackling this first hypothesis was to demonstrate that such an approximation could be achieved with a relatively small energy barrier, coherent with the values calculated from the kinetic experiments. The real process will naturally have an energy barrier even smaller than the one calculated considering our method, due to the natural adjustments of the full enzymatic structure and to the inherent mobility of all residues. However, this aspect does not at all jeopardize the conclusions derived from our method for the problem at hand.

Hence, the factors that justify the approach used of freezing all residues outside a 12 Å radius from the Zn coordination sphere and FPP molecule in FTase can be summed up into four major points: (1) there are no covalent bonds between the FPP and the enzyme, and therefore it is not to be expected that a small conformational change by the FPP would propagate itself to the enzyme in the form of "long-range" conformational rearrangements; (2) the available X-ray structures for the several FTase catalytic intermediates do not exhibit significant conformational changes outside this 12 Å radius active-site region; (3) even if conformational alterations of this type would occur they would only lower the energy barrier, as the reactants are already in the thermal minimum and the products would have to be reverted to such a state; (4) a preliminary attempt to address the FPP conformational change using a fully unconstrained system did not result in alterations at the enzyme backbone, but only in minor rearrangements of the side chains of distant and unrelated residues.

The energy of the several conformations of the FPP molecule was later evaluated outside the enzyme to assess the role of the enzyme. Energy values were calculated at the MM level in vacuum, at the HF/6-31G(d) level (to be consistent with the AMBER parameterization process), and at the B3LYP/6-31G(d) level both in vacuum and in an enzymatic environment (considering a dielectric constant of 4, as discussed in the next section).

Thiolate Displacement Hypothesis

Context

To analyze the thiolate displacement hypothesis an alternative strategy able to accurately characterize in full detail the Zn coordination sphere and the alterations that take place with ligand exit was developed and implemented, by applying high-level quantum calculations. The energy profile for thiolate displacement from

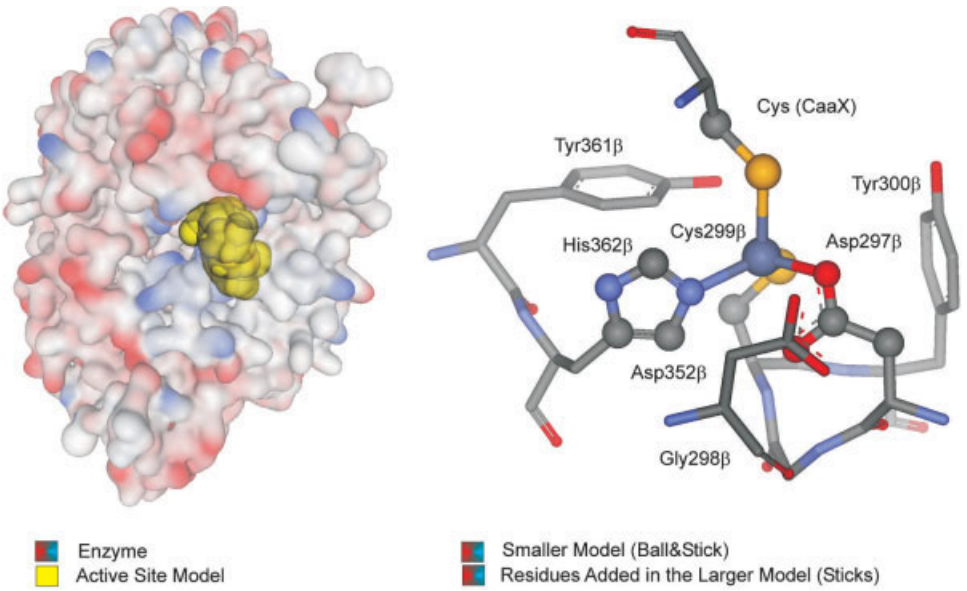

Fig. 3. Farnesyltransferase enzyme. Representation of the 1D8D crystallographic structure (ternary complex),[40] with major emphasis being given to the two models considered in thiolate exit study. [Color figure can be viewed in the online issue, which is available at www.interscience.wiley.com.]

the Zn coordination sphere was evaluated in a first model containing simply the Zn coordination sphere (Smaller Model) and subsequently in a second model that includes also all residues located in a second coordination sphere (Larger Model), as to evaluate the influence of the dimension of the quantum model on the results.

Smaller model

Calculations were performed on an active site model including the zinc ion and all its ligands (Asp297β, Cys299β, His362β, and the peptide thiolate) (Fig. 3). Conventional modeling of the amino acid side chains was used, that is, the zinc ligands aspartate, cysteinate, and histidine were modeled by acetate, methylthiolate, and imidazole, respectively. The validity of this type of approach has been demonstrated before in the mechanistic study of FTase[53,54] and of several different enzymes.[59–65] The model was prepared starting from the 1D8D structure[40], the crystallographic structure of FTase with a peptide substrate and an FPP analog with the highest resolution (2.00 Å).

The geometry of the model was first freely optimized. Subsequently, a scan along the Zn-peptide thiolate sulphur distance was performed. From the electronic energy chart, two minima connected by a transition state were identifiable. The region on the potential energy surface (PES) closer to the maximum was further rescanned at narrower distance intervals, and the maximum subsequently obtained was used as a starting guess to find the correspondent transition state. The transition state structure was later freely optimized. Identical procedure was followed for the final minimum. Frequency analyses were performed at each stationary point on the PES. Therefore, the two minima and the transition state were verified taking in account the number of imaginary frequencies. Zero-point corrections, thermal, and entropic effects (310.15 K, 1 bar) were added to all calculated energies.

In all calculations described above, density functional theory (DFT) with the B3LYP functional[66,67] was used. DFT calculations have been shown to give very accurate results for systems involving transition metals,[68] particularly when using the B3LYP functional.[69–71] Optimizations were carried out using the SDD basis set, as implemented in Gaussian 03.[72] This basis set uses the small core quasi-relativistic Stuttgart/Dresden electron core potentials (also known as Stoll-Preuss, or simply SP)[73,74] for transition elements. For zinc, the outer electrons are described by a (311111/22111/411) valence basis specifically optimized for this metal and for the use with the SP pseudopotentials. C, N, and O atoms are accounted by a (6111/41) quality basis set, whereas S and H atoms are treated respectively by a (531111/4211) and a (31) quality basis sets. The high-performance of SP pseudopotentials in calculations involving transition metals compounds, particularly within closed-shell systems has been previously demonstrated.[75] This basis set has also been used before with B3LYP in the study of FTase.[53,54]

The effect of the long range, nonspecific, isotropic environment was evaluated by considering a polarized continuum model—the IEF-PCM, as implemented in Gaussian 03.[76–79] This model has been shown to give better results for solvents with low dielectric constants than the alternative model C-PCM.[80] This feature is of particular importance to the study of enzymatic catalysis, since the use of a continuum model is normally taken as an approximation to the effect of the global

enzyme environment in a reaction, having been shown in previous studies on active sites in proteins,[59,81,82] that an empirical dielectric constant (ε) of 4 gives generally good agreement with experimental results, and accounts for the average effect of both the protein and buried water molecules. It should be stressed that this treatment of the environment is only valid when the short-range anisotropic interactions are explicitly incorporated in the atomic model (like H-bonds, or ionic enzyme-substrate interactions), as these last cannot be reproduced by the continuum. Therefore, in this study, IEF-PCM calculations were performed using a dielectric constant of 4, in an attempt to reproduce the electrostatic conditions of the enzyme global environment. Previous studies have demonstrated that the effect of the continuum in geometries is, in general, rather small, even in charged systems.[83,84] Therefore, in all PCM calculations, it was assumed that gas-phase geometries could be transferred without the introduction of significant errors. IEF–PCM energy calculations with B3LYP/SDD were performed for both minima, as well as for the transition state. Zero point corrections, thermal, and entropic effects ($T = 310.15$ K, $P = 1$ bar) were added to all calculated energies, as well.

Larger model

In an attempt to analyze the influence of the enzyme environment on the zinc coordination sphere and on thiolate displacement, a significant enlargement of the model size was made. Calculations were performed on a 119 atoms active site model (designated Larger Model), based on an 8 Å cut around the zinc atom in the 1D8D structure (Fig. 3), and comprised the earlier model plus four complete residues (Gly298β, Tyr300β, Asp352β, and Tyr361β) treated at the B3LYP/SDD level of theory. The overall procedure described in the treatment of the smaller model was again used. The only exception was the optimization process, where the two layers ONIOM approach,[85,86] as implemented in Gaussian 03, was followed using B3LYP/SDD in the inner layer (defined in analogy with the smaller model, size 23 atoms) and PM3[87–89] in the outer layer (the four new residues added, size 96 atoms). The geometry of the model was first freely optimized. A scan along the Zn-peptide thiolate sulphur distance was performed, as described for the small model. The energy of the bound minimum and of the transition state-like structure was also evaluated in continuum (IEF-PCM model), considering a dielectric constant of 4 and using B3LYP/SDD in the treatment of the entire system. This approach has also been previously used with success in the study of FTase.[53,54]

RESULTS AND DISCUSSION

The Distances Paradox

Despite the vast interest surrounding FTase, several key features in the farnesylation mechanism remain unexplained. The structure of the productive ternary complex (FTase-FPP-peptide) represents, most probably, one of the most interesting and appealing unsettled aspects in FTase research. Even though various X-ray crystallographic structures for the ternary complex exist, all of these structures include components (substrate analogues) which are catalytically inactive, and therefore represent non productive conformations (FTase-FPP-peptide analogue or FTase-FPP analogue-peptide). One of the most puzzling features which arises from these structures is the very large distance (over 7 Å) reported between the two reactive atoms in the farnesylation reaction namely the FPP C1 and the thiolate sulfur.[39–41] This distance must be overcome for the alkylation reaction to occur, which implies a rearrangement of at least one of the two substrates for the formation of the reactive intermediate.

There are basically three alternatives by which a substrate rearrangement with concomitant FPP C1 thiolate sulfur approach could be achieved. The first logical hypothesis would involve a major conformational change of the enzyme environment, which would bring together both substrates. The second alternative would implicate thiolate dissociation from zinc, with simultaneous translocation nearer to FPP.[42–44] Finally, the third possibility would comprehend a movement of the FPP C1 towards the zinc-bound peptide thiolate, possibly through a rotation involving the first two isoprene subunits.[45,46]

An analysis of the several crystallographic structures available along the reaction coordinate[46] has pointed out the existence of only, rather localized structural rearrangements, involving solely the substrates and some directly interacting amino acid side chains. These conclusions are not coherent with a major enzymatic rearrangement, and hence, the first hypothesis is not feasible.

More recently, some evidence consistent with the FPP rotation hypothesis were presented. In fact, an explanation for the conformational differences of the FPP molecule in the X-ray crystallographic structures of the ternary and product complexes was suggested, admitting a rotation of the first two isoprene subunits.[46] A rearrangement, such as the one proposed, could bring together both reactants to a distance of 2.4 Å, sufficient for the reaction to occur.[45] Additionally, mutagenesis studies performed on residues Lys164α, H248β, and Tyr300β have resulted in alterations on the FPP reactivity that are coherent with the change in diphosphate moiety position that would be expected with FPP rotation.[45] However, although the FPP rotation hypothesis is currently considered, the most likely option, the thiolate dissociation alternative remains a reasonable possibility, not yet ruled out. Understanding the true nature of this enigma, would not only represent a major step in the search for the elusive structure of the productive intermediate, but would also have a remarkable impact in the knowledge of the farnesylation mechanism itself.

The FPP Rotation Hypothesis

CVIM peptide substrate

We started our study by evaluating if the FPP conformational change postulated from experimental data was

at all feasible. Our calculations for the FPP rotation considering the Zn-bound CVIM peptide substrate, starting from the fully energy minimized system (Structure **I**, Fig. 4), resulted in a regular energy increase until 10 kcal/mol (Structure **II**), followed by a plateau that goes up to a 5.45 Å distance between the two reactive atoms (Structure **III**). From this point onwards, the energy increases steadily until the two reactive atoms enter in van der Waals contact (Structure **IV**). The energy continues to increase for closer distances until 95 kcal/mol (Structure **V**). Beyond this point no convergence is achieved.

An analysis of the intermediate structures presented in Figure 4 reveals interesting structural trends accompanying the FPP conformational change. In addition to the pyrophosphate moiety, the FPP molecule comprises a total of 15 carbon atoms, distributed by three isoprenoid subunits. Our results show that the conformational change that brings the two reactive atoms into contact can take place without any change of FPP Subunit 3 (Fig. 4) and with a very moderate rotation by Subunit 2. Subunit 1, containing the FPP C1, supports the bulk of the conformational changes, as suggested from experiment.[45] The position of the pyrophosphate moiety is strongly stabilized by hydrogen bonds between the pyrophosphate terminal oxygens and the amino acid residues Lys164α, Arg291β, and Lys294β and does not change appreciably during the entire process. The importance of these interactions in FPP stabilization has been highlighted before in previous structural[39,90,91] and mutagenesis[42,45,51,92,93] studies. Our results show that the positions of these residues are maintained throughout the FPP conformational change. Moreover, from our results, it is visible that the FPP conformational change between structures **I** and **IV** does not significantly alter the hydrogen bonds between the pyrophosphates nonbridging oxygens and the two lysines (Lys164α and Lys294β). However, this is not the case for Arg291β. Although the hydrogen bonds of this residue with the oxygen atoms on the β-phosphate of the FPP molecule are very well maintained during the FPP conformational change, the hydrogen bond to one of the oxygen atoms on the α-phosphate experiences significant changes that, parallel with the energy profile that takes place. This bond suffers a 0.12 Å increase between structures **I** and **II**, when the energy changes by 10 kcal/mol. From structure **II** to **III,** the energy is maintained and this bond does not change appreciably. From structure **III** onwards, both the energy and the length of this hydrogen bond increase steadily (by as much as 30 kcal/mol and 0.30 Å respectively, for structure **IV**). Finally, for structure **V,** where the two reactive atoms are at a 2.65 Å distance, this hydrogen bond is totally disrupted and the energy reaches 95 kcal/mol.

Overall, the change between structures **I** and **II** is characterized by a small rotation of Subunit 1 with an energetic cost of 10 kcal/mol that brings the two reactive atoms from a distance of 7.23–6.35 Å, and induces the weakening of a critical hydrogen bond between Arg291β and one of the FPP α-phosphate oxygens. From structures **II** to **III**, the Subunit 1 continues to rotate approaching the FPP C1 to a 5.45-Å distance from the Zn-bound peptide thiolate, without significant change on the length of any of the hydrogen bonds involving the pyrophosphate moiety and with very moderate changes on the angles of these hydrogen-bonds, and on the energy of the system. The change between structures **III** and **IV** is characterized by rotation of the FPP molecule that involves also Subunit 2, leading the two reactive atoms to a 4.05-Å distance. This change is accompanied by a regular increase in energy and a 0.3 increase in the critical hydrogen bond to Arg291β. Beyond structure **IV** and until structure **V** the two reactive atoms enter in van der Waals contact (C—S pairwise van der Waals radius 4.0 Å); the energy increases by 55 kcal/mol and the hydrogen bonds to Lys164α, Arg291β, and Lys294β are completely altered.

Figure 4 also illustrates the energy of the individual FPP molecule in each of the conformations formed. Values were calculated at the MM level in vacuum, and at the HF/6-31G(d) level to be consistent with the AMBER parameterization process. Subsequently, B3LYP/6-31G(d) calculations were also performed for each state. The latter calculations in HF and B3LYP were performed in vacuum and in a nonspecific enzymatic environment (represented by a dielectric constant of 4). The results show that the energy barrier that corresponds to the FPP conformational change discussed above (up to a 5.4 Å C1—S distance) has an energy slightly higher for the free molecule in the five types of calculations performed in the enzyme. This indicates that the FPP conformational change is stabilized in the enzyme by specific residues in the active site. Furthermore, the values observed for the FPP conformational change all fall below a 30 kcal/mol limit (with just two exceptions). This further confirms that the energy increase observed in the enzyme from a 5.4 Å distance onwards relates to the enzyme-FPP interaction, and does not arise from the FPP molecule itself.

Kinetic studies have demonstrated that for the transformation from the ternary complex to the product complex in FTase (which includes the conformational change to the productive intermediate and the chemical step) the rate constant is of 17 s^{-1}.[48] According to the transition state theory, this value corresponds to a Gibbs activation energy of ~16 kcal/mol. Our results show that a rotation involving Subunits 1 and 2 of the FPP substrate can take place inside the FTase active site, leading to an approach between the two reactive atoms from 7.3 to 5.4 Å, significantly below the experimental 16 kcal/mol limit. The subsequent increase in energy, for distances smaller than 5.4 Å, is in agreement with the beginning of the chemical step, when bond breaking and bond making processes start, and MM methods that use harmonic potentials are unable to describe the events taking place. These include the breaking of the disphosphate–C1 bond, the making of the C1—S bond, the breaking of the Zn—S bond, and a carboxylate-shift

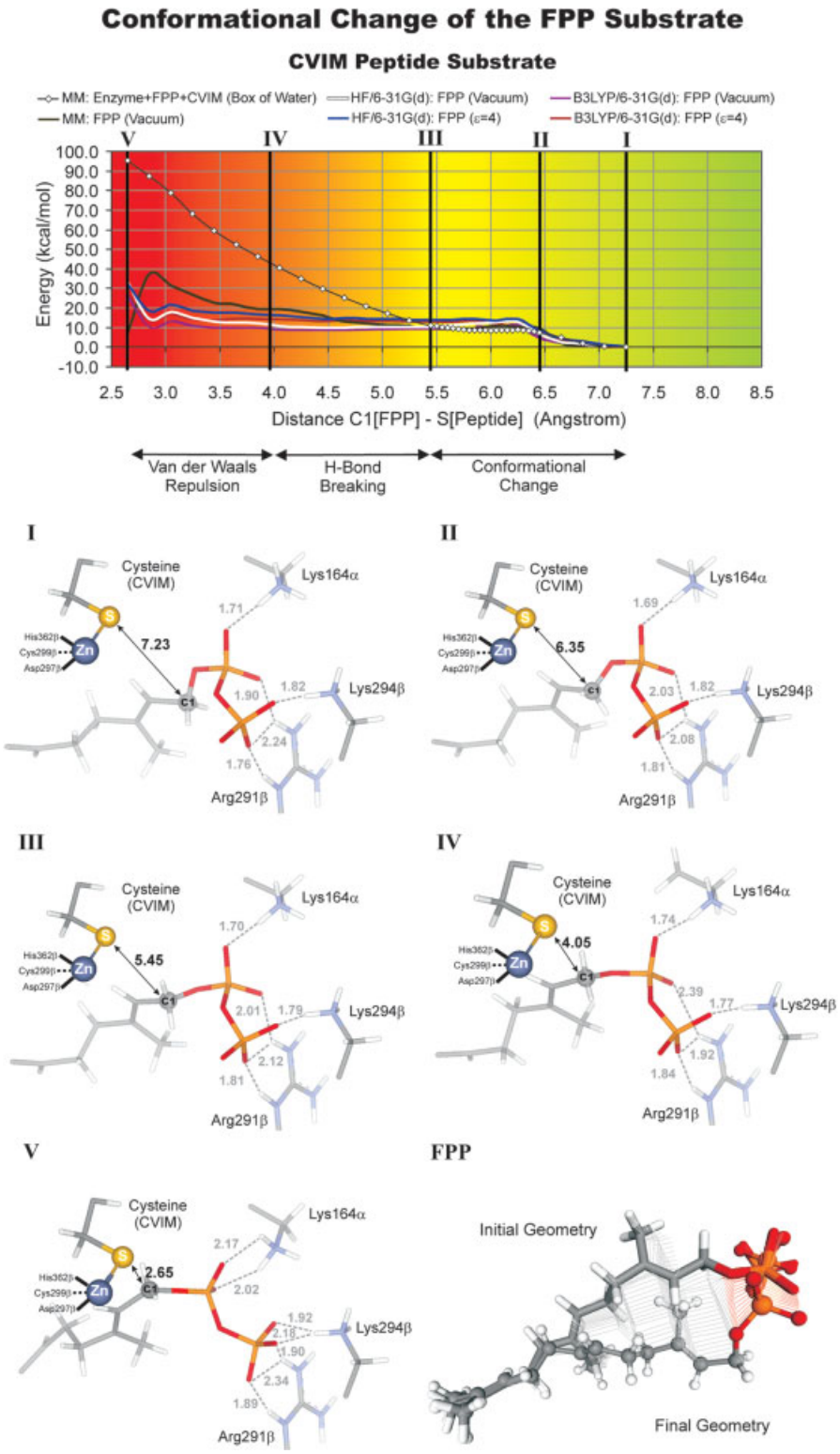

Fig. 4. MM energy profile for the FPP conformational change with the CVIM peptide substrate in the enzyme, and single FPP energy values in MM in vacuum, HF/6-31G(d) in vacuum, and HF/6-31G(d) in an enzymatic environment ($\varepsilon = 4$), B3LYP/6-31G(d) in vacuum, and B3LYP/6-31G(d) in an enzymatic environment ($\varepsilon = 4$). Schematic representations of the five key intermediate structures formed during the process and of the FPP intermediate structures formed during the process. [Color figure can be viewed in the online issue, which is available at www.interscience.wiley.com.]

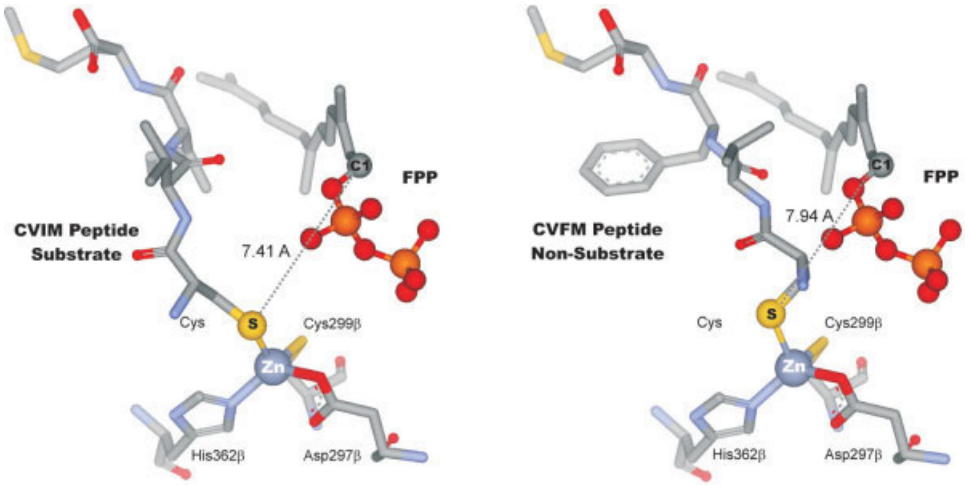

Fig. 5. The different coordination modes for a CVIM substrate peptide and a CVFM nonsubstrate peptide. Enzyme structures taken from the 1JCR crystallographic structure (ternary complex FTase-FPP-CVFM, resolution 2.00 Å). CVIM peptide structure taken from the 1D8D crystallographic structure (ternary complex FTase-FPP analog-CVIM, resolution 2.00 Å) and modeled into the 1JCR crystallographic structure. [Color figure can be viewed in the online issue, which is available at www.interscience.wiley.com.]

change by Asp297β (monodentate to bidentate). The role of a catalytically very relevant Mg^{2+} cation, thought to assist the full process by interacting with the diphosphate group further complicates the problem. Therefore, it is not surprising that the order and full extension of the processes taking place in this chain of events remain a matter of great dispute.[38]

CVFM peptide inhibitor

Some CaaX tetrapeptides have been shown to act as inhibitors by coordinating through a nonsubstrate binding mode. Conformation mapping calculations have demonstrated that it is the third position of the CaaX motif that determines whether a tetrapeptide acts as a substrate or an inhibitor.[41] The presence of a β-branched amino acid at this position prevents formation of the nonsubstrate conformation; the presence of any other aliphatic amino acid has been predicted to form nonsubstrate conformations.[41,94,95] The CVIM substrate studied above coordinates in an extended conformation,[39,40] whereas the CVFM peptide coordinates in a β-turn nonsubstrate conformation.[41,96]

As an explanation for the observed difference in terms of activity, it has long been proposed that the conformation in which the nonsubstrate peptides bind might preclude farnesyl transfer from the FPP substrate to the peptidic thiolate by preventing some crucial conformational change on the enzyme.[97] To check the validity of this hypothesis, we have analyzed the behavior of the CVFM peptide with the FPP conformational change, and have compared it with the results obtained for the CVIM substrate (Fig. 5).

For the CVFM peptide inhibitor, our calculations for the FPP rotation, starting from the fully energy minimized system (Structure **I**, Fig. 6), resulted in a plateau that goes up to a 7.11 Å between the two reactive atoms (Structure **II**), followed by a steady energy increase until 22 kcal/mol (Structure **III**), a point where the FPP C1 enters in van der Waals contact with the β-carbon from the Zn-bound cysteine (C—C pairwise van der Waals radius 4.0 Å). From this point onwards, the energy raises steeper until a 4.91 Å distance between the two reactive atoms is reached (Structure **IV**). Beyond this point no convergence is achieved.

An analysis of the intermediate structures, presented in Figure 6, reveals remarkable similarities with the CVIM peptide in terms of hydrogen-bonding patterns throughout the FPP conformational change, in agreement with the fact that FPP substrate binding to the enzyme takes place before peptide coordination,[48,98–100] and hence may be regarded as independent.

Our results show that with the CVFM peptide inhibitor, the FPP conformational change between structures **I** and **IV** does not significantly alter the hydrogen bonds between the pyrophosphate hydrogens and the amino acid residues Lys164α, Arg291β, and Lys294β, with the exception of the hydrogen bond between Arg291β and one the oxygen atoms on the α-phosphate, as reported for the CVIM peptide. However, our results demonstrate that the energy profile for the FPP conformational change with the CVFM peptide inhibitor is significantly altered in relation to the one calculated considering a CVIM peptide substrate, with a continuous raise in energy. Moreover, our results show that this difference in terms of energy is a direct consequence of the different coordination mode adopted by the CaaX peptides. The coordination mode of the CVFM peptide inhibitor prevents FPP C1 approach from the Zn bound thiolate sulphur atom, as the cysteine β- and α-carbons and the correspondent hydrogen atoms completely block the path.

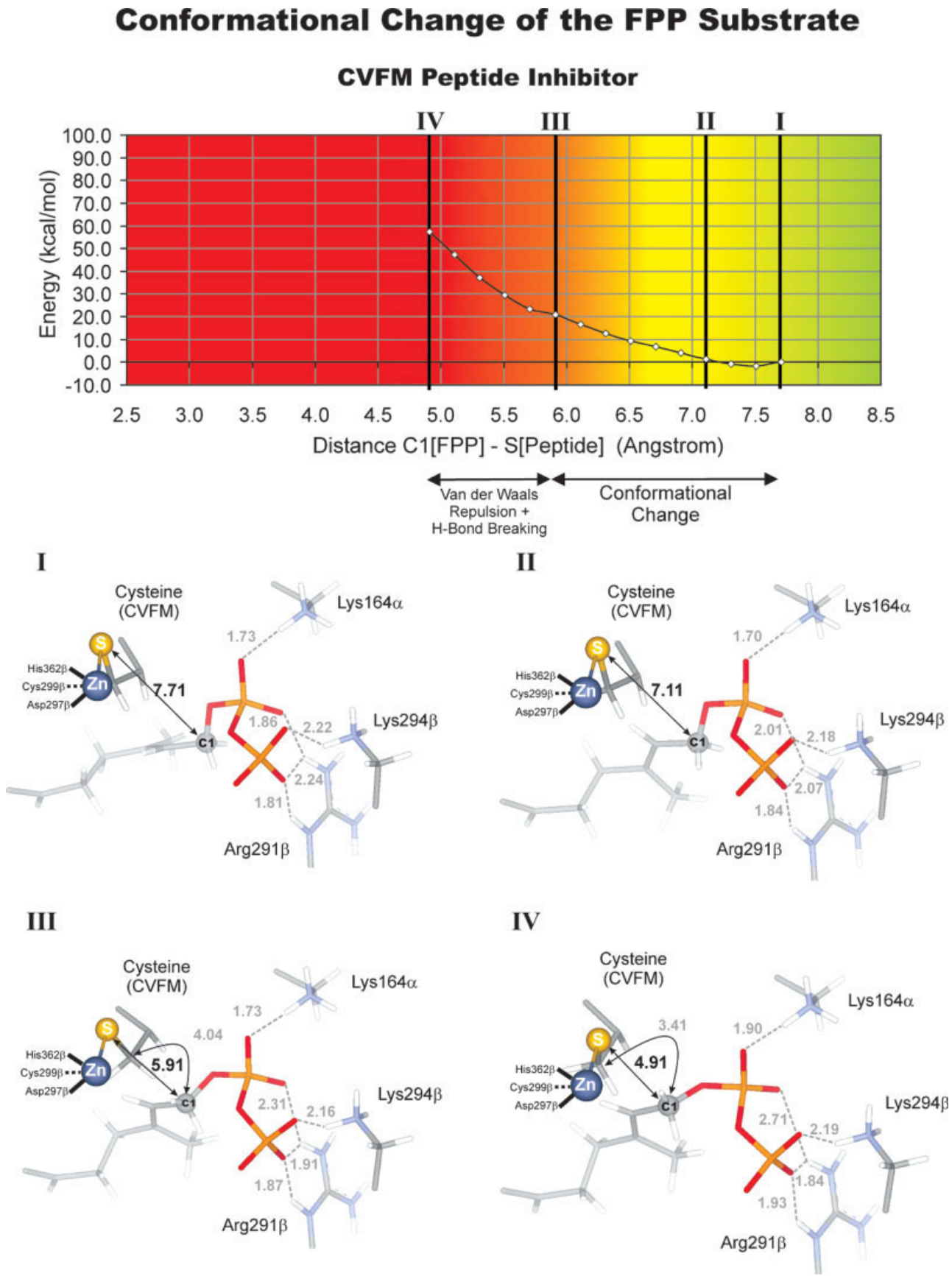

Fig. 6. Energy profile for the FPP conformational change with the CVFM peptide inhibitor. Schematic representations of the four key intermediates structures formed during the process. [Color figure can be viewed in the online issue, which is available at www.interscience.wiley.com.]

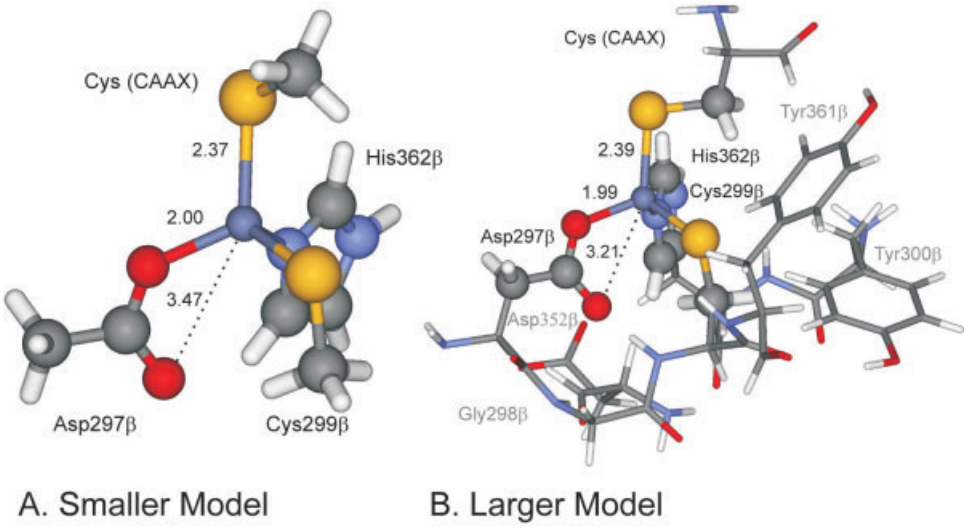

Fig. 7. Structures of the zinc coordination spheres in the ternary complexes for the smaller and larger models.

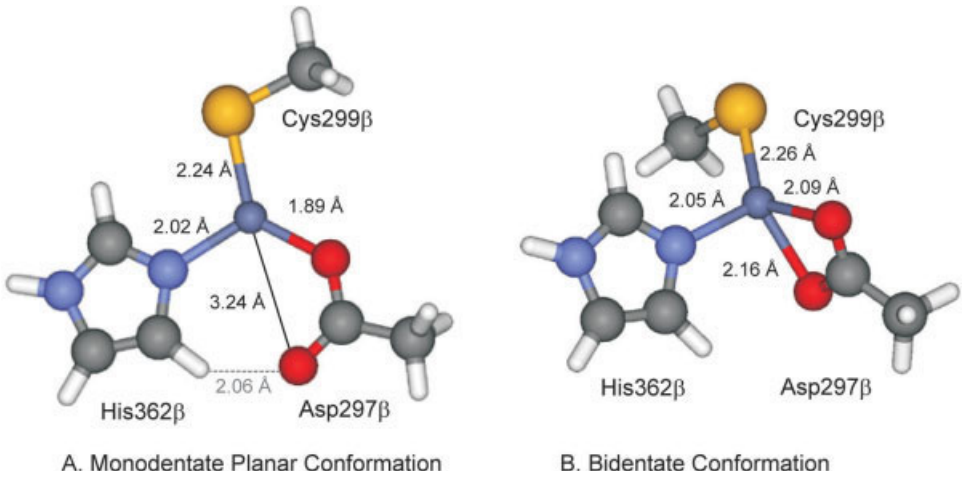

Fig. 8. Monodentate planar and bidentate conformations, resulting from thiolate substrate exit in the smaller model. The planar structure is more stable by 2.7 kcal/mol.

Altogether, the MM studies performed demonstrate that a rotation of Subunits 1 and 2 of the FPP substrate can effectively lead to an approach of the two reactive atoms with an energetic cost coherent with experiment, and that this conformational change further correlates in terms of activity with the different behavior exhibited by different CaaX peptides.

The Thiolate Displacement Hypothesis

At a later stage, we have analyzed a possible displacement of the peptide thiolate from the zinc coordination sphere, in order to evaluate if a thiolate departure from the metal sphere towards the FPP could be a realistic hypothesis of overcoming the very large distance reported between the two reactive atoms in the farnesylation reaction between thiolate sulfur atom and FPP C1. Two models of different sizes were considered (Fig. 3). The preparation of the larger model was carefully planned to capture both the intrinsic characteristic of the zinc complex and the influence of the anisotropic enzyme environment on the zinc coordination sphere. This type of model has been used with success in the mechanistic study of FTase[53,54] and several other enzymes.[101–104] All residues interacting directly with the zinc ligands were included to preserve the specific interactions of the enzyme environment with the metal coordination sphere. Special care was taken to include all the hydrogen bonds between the zinc ligands and the surrounding residues. The remaining portion of FTase, not included in the larger model, was replaced by a dielectric continuum ($\varepsilon = 4$), which is a standard procedure in the treatment of the long-range nonspecific effects of the enzyme environment.[59,62,81,82] Therefore, the conclusions drawn from this model can be extrapolated for the enzymatic system. Obviously, our model is

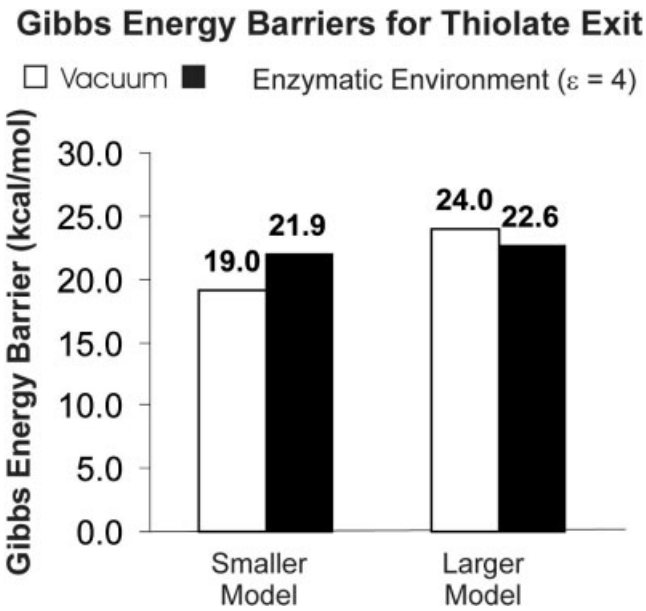

Fig. 9. Gibbs energy barriers for thiolate substrate displacement from the zinc coordination sphere, considering the smaller and larger models.

not complete enough to allow a characterization of a minimum formed after ligand elimination, nor pretends to be. This work focuses on the active-site zinc coordination sphere, and on the structural and energetic alterations caused by ligand exit. In this regard, the second layer of residues included assures a realistic treatment of the geometry of the metal coordination sphere. Hence, our larger model allows a very reasonable estimate of the potential energy barriers, which result from ligand displacement from the metal coordination sphere, a strategy already applied earlier with success in the study of FTase.[53,54] A subsequent enlargement of the atomistic region in our models, even though it could greatly benefit the treatment of the minima resulting from ligand exit, would not bring significant advantages to the characterization of the zinc coordination sphere or to the evaluation of the energy barriers for ligand exit from the metal sphere. The main purpose of considering also the first smaller model was to discriminate between the intrinsic characteristics of the zinc complex and the influence of the enzyme. This can be achieved by comparing the results of the two models, whose differences can be fully attributed to the enzyme specific interactions that arise from the residues surrounding the Zn coordination sphere.

The geometry of the zinc coordination sphere in the starting minima, obtained for both models, is represented in Figure 7. The zinc–peptide bond-lengths obtained for the smaller and larger models were respectively of 2.37 and 2.39 Å, very close to the 2.40 Å value reported in the 1D8D crystallographic structure.[40] EXAFS studies[47] indicate an average value for the two thiolate bonds (with the peptide substrate and Cys299β) of 2.33 E, also in agreement with the average values indicated by our models, 2.36 Å (smaller model) and 2.39 Å (larger model). In the larger model, the overall conformation of the residues surrounding the active site was maintained in relation to the 1D8D crystallographic structures (without any constraint having been applied), whereas for the smaller model some natural deviations were observed.

The study performed has demonstrated that the four residues surrounding the zinc coordination sphere are absolutely vital in the stabilization of a conformation formed with ligand exit, where Asp297β is bidentate. In fact, with the use of the smaller model, ligand departure resulted not in the bidentate minimum but in an absolutely planar conformation (Fig. 8). Our study has shown that the energy difference between both conformations is small, with the bidentate minimum at an energy 2.7 kcal/mol higher. In the larger model the geometric constrains, which arise from the inclusion of the residues surrounding the metal coordination sphere, hinder a conformational change to a planar minimum. Hence, in the enzyme only the bidentate minimum exists after ligand elimination.

The values suggested by our study for a thiolate displacement from the zinc coordination sphere clearly exceed the values calculated from experiment for the chemical step (~16 kcal/mol),[48] varying from 21.9 kcal/mol in the smaller model, to 22.6 kcal in the larger model (Fig. 9). It is worth noticing that this larger model does not take into consideration all the interactions of the substrate peptide (a tetrapeptide) that would have to be destroyed with thiolate displacement, and only accounts for the most important ones, which arise from zinc and closer residues. Hence, the calculated values are only partial and the true values are expected to be even higher. Therefore, a displacement of the peptide substrate thiolate from the zinc coordination sphere to the FPP C1 is not a realistic alternative of overcoming the 7-Å distance reported in the crystallographic structures between the two reactive atoms in FTase. This shows that in FTase the peptide thiolate cannot possibly leave the zinc coordination sphere prior to the chemical step. Hence, the only feasible alternative of bringing together the two reactive atoms is through an FPP rearrangement.

CONCLUSIONS

The results obtained in this study reveal that in FTase a displacement of the peptide substrate thiolate from the zinc coordination sphere towards the FPP C1 is not a realistic alternative to bring together the two reactive atoms, which have been shown to lay more than 7 Å apart in the available crystallographic structures of the ternary complex. In fact, the calculated energy barrier for thiolate exit is significantly higher than the one determined from kinetic studies for the rate limiting step in the farnesylation reaction, demonstrating that the peptide thiolate cannot leave the zinc coordination sphere prior to the chemical step. Our results have also

demonstrated that a rotation involving Subunits 1 and 2 of the FPP molecule can bring the two reactive atoms to a suitable distance for the chemical step to take place. Furthermore, our results have shown that such a movement can take place in the active-site of FTase with a moderate energetic cost, coherent with previous experimental data. Substitution of a peptide substrate CVIM by a nonsubstrate peptide inhibitor CVFM blocks the FPP conformational change, as proposed from experiment. These conclusions definitively solve the "distances paradox", one of the most fundamental dilemmas in the elusive catalytic mechanism of the puzzling FTase enzyme, opening the door to an understanding of the complex chemical step in the farnesylation reaction, where several steps are expected to take place in a concerted fashion.

REFERENCES

1. Chen WJ, Andres DA, Goldstein JL, Russell DW, Brown MS. cDNA cloning and expression of the peptide-binding β-subunit of rat p21ras farnesyltransferase, the counterpart of yeast DPR1/RAM1. Cell 1991;66:327–334.
2. Chen WJ, Andres DA, Goldstein JL, Brown MS. Cloning and expression of a cDNA-encoding the α subunit of rat p21ras protein farnesyltransferase. Proc Natl Acad Sci USA 1991;88: 11368–11372.
3. Moores SL, Schaber MD, Mosser SD, Rands E, O'Hara MB, Garsky VM, Marshall MS, Pompliano DL, Gibbs JB. Sequence dependence of protein isoprenylation. J Biol Chem 1991;266: 14603–14610.
4. Reiss Y, Goldstein JL, Seabra MC, Casey PJ, Brown MS. Inhibition of purified p21ras farnesyl: protein transferase by Cys-AAX tetrapeptides. Cell 1990;62:81–88.
5. Reiss Y, Seabra MC, Armstrong SA, Slaughter CA, Goldstein JL, Brown MS. Nonidentical subunits of p21H-ras farnesyltransferase. Peptide binding and farnesyl pyrophosphate carrier functions. J Biol Chem 1991;266:10672–10677.
6. Schafer WR, Rine J. Protein prenylation—genes, enzymes, targets, and functions. Annu Rev Genet 1992;26:209–237.
7. Glomset JA, Farnsworth CC. Role of protein modification reactions in programming interactions between ras-related GTPases and cell membranes. Annu Rev Cell Biol 1994;10: 181–205.
8. Zhang FL, Casey PJ. Protein prenylation: molecular mechanisms and functional consequences. Annu Rev Biochem 1996; 65:241–269.
9. Hancock JF, Magee AI, Childs JE, Marshall CJ. All ras proteins are polyisoprenylated but only some are palmitoylated. Cell 1989;57:1167–1177.
10. Jackson JH, Cochrane CG, Bourne JR, Solski PA, Buss JE, Der CJ. Farnesol modification of Kirsten-ras exon 4B protein is essential for transformation. Proc Natl Acad Sci USA 1990;87:3042–3046.
11. Kato K, Cox AD, Hisaka MM, Graham SM, Buss JE, Der CJ. Isoprenoid addition to ras protein is the critical modification for its membrane association and transforming activity. Proc Natl Acad Sci USA 1992;89:6403–6407.
12. Dolence JM, Poulter CD. A mechanism for posttranslational modifications of proteins by yeast protein farnesyltransferase. Proc Natl Acad Sci USA 1995;92:5008–5011.
13. James G, Goldstein JL, Brown MS. Resistance of K-RasBV12 proteins to farnesyltransferase inhibitors in rat1 cells. Proc Natl Acad Sci USA 1996;93:4454–4458.
14. Takai Y, Sasaki T, Matozaki T. Small GTP-binding proteins. Physiol Rev 2001;81:153–208.
15. Ayral-Kaloustian S, Salaski EJ. Protein farnesyltransferase inhibitors. Curr Med Chem 2002;9:1003–1032.
16. Ohkanda J, Knowles DB, Blaskovich MA, Sebti SM, Hamilton AD. Inhibitors of protein farnesyltransferase as novel anticancer agents. Curr Top Med Chem 2002;2:303–323.
17. Brunner TB, Hahn SM, Gupta AK, Muschel RJ, McKenna WG, Bernhard EJ. Farnesyltransferase inhibitors: an overview of the results of preclinical and clinical investigations. Cancer Res 2003;63:5656–5668.
18. Caponigro F, Casale M, Bryce J. Farnesyltransferase inhibitors in clinical development. Expert Opin Investig Drugs 2003; 12:943–954.
19. Doll RJ, Kirschmeier P, Bishop WR. Farnesyltransferase inhibitors as anticancer agents: critical crossroads. Curr Opin Drug Discov Dev 2004;7:478–486.
20. Adjei AA. Farnesyltransferase inhibitors. Cancer Chemother Biol Response Modif 2005;22:123–133.
21. Kurzrock R. Farnesyltransferase inhibitors. Clin Adv Hematol Oncol 2005;3:161–162.
22. Appels NMGM, Beijnen JH, Schellens JHM. Development of farnesyltransferase inhibitors: a review. Oncologist 2005;10: 565–578.
23. Huang CY, Rokosz L. Farnesyltransferase inhibitors: recent advances. Expert Opin Ther Patents 2004;14:175–186.
24. Chakrabarti D, Da Silva T, Barger J, Paquette S, Patel H, Patterson S, Allen CM. Protein farnesyltransferase and protein prenylation in *Plasmodium falciparum*. J Biol Chem 2002;277:42066–42073.
25. Wiesner J, Kettler K, Sakowski J, Ortmann R, Katzin A, Kimura E, Silber K, Klebe G, Jomaa H, Schlitzer M. Farnesyltransferase inhibitors inhibit the growth of malaria parasites in vitro and in vivo. Angew Chem Int Ed Engl 2004;43:251–254.
26. Kettler K, Wiesner J, Silber K, Haebel P, Ortmann R, Sattler I, Dahse HM, Jomaa H, Klebe G, Schlitzer M. Non-thiol farnesyltransferase inhibitors: *N*-(4-aminoacylamino-3-benzoylphenyl)-3-[5-(4-nitrophenyl)-2 furyl]acrylic acid amides and their antimalarial activity. Eur J Med Chem 2005;40:93–101.
27. Eastman RT, White J, Hucke O, Bauer K, Yokoyama K, Nallan L, Chakrabarti D, Verlinde CLMJ, Gelb MH, Rathod PK, Van Voorhis WC. Resistance to a protein farnesyltransferase inhibitor in *Plasmodium falciparum*. J Biol Chem 2005;280: 13554–13559.
28. Glenn MP, Chang SY, Hucke O, Verlinde CL, Rivas K, Horney C, Yokoyama K, Buckner FS, Pendyala PR, Chakrabarti D, Gelb M, Van Voorhis WC, Sebti SM, Hamilton AD. Structurally simple farnesyltransferase inhibitors arrest the growth of malaria parasites. Angew Chem Int Ed Engl 2005;44:4903–4906.
29. Nallan L, Bauer KD, Bendale P, Rivas K, Yokoyama K, Horney CP, Pendyala PR, Floyd D, Lombardo LJ, Williams DK, Hamilton A, Sebti S, Windsor WT, Weber PC, Buckner FS, Chakrabarti D, Gelb MH, Van Voorhis WC. Protein farnesyltransferase inhibitors exhibit potent antimalarial activity. J Med Chem 2005;48:3704–3713.
30. Yokoyama K, Trobridge P, Buckner FS, Van Voorhis WC, Stuart KD, Gelb MH. Protein farnesyltransferase from *Trypanosoma brucei*. A heterodimer of 61- and 65-kda subunits as a new target for antiparasite therapeutics. J Biol Chem 1998; 273:26497–26505.
31. Buckner FS, Yokoyama K, Nguyen L, Grewal A, Erdjument-Bromage H, Tempst P, Strickland CL, Xiao L, Van Voorhis WC, Gelb MH. Cloning, heterologous expression, and distinct substrate specificity of protein farnesyltransferase from *Trypanosoma brucei*. J Biol Chem 2000;275:21870–21876.
32. Ohkanda J, Buckner FS, Lockman JW, Yokoyama K, Carrico D, Eastman R, Luca-Fradley K, Davies W, Croft SL, Van Voorhis WC, Gelb MH, Sebti SM, Hamilton AD. Design and synthesis of peptidomimetic protein farnesyltransferase inhibitors as anti-*Trypanosoma brucei* agents. J Med Chem 2004;47:432–445.
33. Buckner FS, Eastman RT, Nepomuceno-Silva JL, Speelmon EC, Myler PJ, Van Voorhis WC, Yokoyama K. Cloning, heterologous expression, and substrate specificities of protein farnesyltransferases from *Trypanosoma cruzi* and *Leishmania major*. Mol Biochem Parasitol 2002;122:181–188.
34. Esteva MI, Kettler K, Maidana C, Fichera L, Ruiz AM, Bontempi EJ, Andersson B, Dahse HM, Haebel P, Ortmann R, Klebe G, Schlitzer M. Benzophenone-based farnesyltransferase inhibitors with high activity against *Trypanosoma cruzi*. J Med Chem 2005;48:7186–7191.

35. Hucke O, Gelb MH, Verlinde CL, Buckner FS. The protein farnesyltransferase inhibitor Tipifarnib as a new lead for the development of drugs against Chagas disease. J Med Chem 2005;48:5415–5418.
36. Ibrahim M, Azzouz N, Gerold P, Schwarz RT. Identification and characterisation of *Toxoplasma gondii* protein farnesyltransferase. Int J Parasitol 2001;31:1489–1497.
37. Bordier BB, Ohkanda J, Liu P, Lee SY, Salazar FH, Marion PL, Ohashi K, Meuse L, Kay MA, Casey JL, Sebti SM, Hamilton AD, Glenn JS. In vivo antiviral efficacy of prenylation inhibitors against hepatitis δ virus. J Clin Invest 2003;112: 407–414.
38. Sousa SF, Fernandes PA, Ramos MJ. Unraveling the mechanism of the farnesyltransferase enzyme. J Biol Inorg Chem 2005;10:3–10.
39. Strickland CL, Windsor WT, Syto R, Wang L, Bond R, Wu Z, Schwartz J, Le HV, Beese LS, Weber PC. Crystal structure of farnesyl protein transferase complexed with a CaaX peptide and farnesyl diphosphate analogue. Biochemistry 1998;37: 16601–16611.
40. Long SB, Casey PJ, Beese LS. The basis for K-Ras4B binding specificity to protein farnesyltransferase revealed by 2 Å resolution ternary complex structures. Structure Fold Des 2000; 8:209–222.
41. Long SB, Hancock PJ, Kral AM, Hellinga HW, Beese LS. The crystal structure of human protein farnesyltransferase reveals the basis for inhibition by CaaX tetrapeptides and their mimetics. Proc Natl Acad Sci USA 2001;98:12948–12953.
42. Wu Z, Demma M, Strickland CL, Radisky ES, Poulter CD, Le HV, Windsor WT. Farnesyl protein transferase: identification of K164 α and Y300 β as catalytic residues by mutagenesis and kinetic studies. Biochemistry 1999;38:11239–11249.
43. Rozema DB, Poulter CD. Yeast protein farnesyltransferase. pKas of peptide substrates bound as zinc thiolates. Biochemistry 1999;38:13138–13146.
44. Harris CM, Derdowski AM, Poulter CD. Modulation of the zinc(II) center in protein farnesyltransferase by mutagenesis of the zinc(II) ligands. Biochemistry 2002;41:10554–10562.
45. Pickett JS, Bowers KE, Hartman HL, Fu HW, Embry AC, Casey PJ, Fierke CA. Kinetic studies of protein farnesyltransferase mutants establish active substrate conformation. Biochemistry 2003;42:9741–9748.
46. Long SB, Casey PJ, Beese LS. Reaction path of protein farnesyltransferase at atomic resolution. Nature 2002;419:645–650.
47. Tobin DA, Pickett JS, Hartman HL, Fierke CA, Penner-Hahn JE. Structural characterization of the zinc site in protein farnesyltransferase. J Am Chem Soc 2003;125:9962–9969.
48. Furfine ES, Leban JJ, Landavazo A, Moomaw JF, Casey PJ. Protein farnesyltransferase: kinetics of farnesyl pyrophosphate binding and product release. Biochemistry 1995;34:6857–6862.
49. Fu HW, Beese LS, Casey PJ. Kinetic analysis of zinc ligand mutants of mammalian protein farnesyltransferase. Biochemistry 1998;37:4465–4472.
50. Pickett JS, Bowers KE, Fierke CA. Mutagenesis studies of protein farnesyltransferase implicate aspartate β 352 as a magnesium ligand. J Biol Chem 2003;278:51243–51250.
51. Bowers KE, Fierke CA. Positively charged side chains in protein farnesyltransferase enhance catalysis by stabilizing the formation of the diphosphate leaving group. Biochemistry 2004;43:5256–5265.
52. Hartman HL, Bowers KE, Fierke CA. Lysine β 311 of protein geranylgeranyltransferase type I partially replaces magnesium. J Biol Chem 2004;279:30546–30553.
53. Sousa SF, Fernandes PA, Ramos MJ. Farnesyltransferase—new insights into the zinc-coordination sphere paradigm: evidence for a carboxylate-shift mechanism. Biophys J 2005;88: 483–494.
54. Sousa SF, Fernandes PA, Ramos MJ. Farnesyltransferase: theoretical studies on peptide substrate entrance—thiol or thiolate coordination? J Mol Struct (Theochem) 2005;729:125–129.
55. Case DA, Darden TA, Cheatham TE, III, Simmerling CL, Wang J, Duke RE, Luo R, Merz KM, Wang B, Pearlman DA, Crowley M, Brozell S, Tsui V, Gohlke H, Mongan J, Hornak V, Cui G, Beroza P, Schafmeister C, Caldwell JW, Ross WS, Kollman PA. AMBER 8. San Francisco: University of California; 2004.
56. Sousa SF, Fernandes PA, Ramos MJ. Effective tailor-made force field parameterization of the several Zn coordination environments in the puzzling FTase enzyme: opening the door to the full understanding of its elusive catalytic mechanism. Theor Chem Acc, in press.
57. Essman V, Perera L, Berkowitz ML, Darden T, Lee H, Pedersen LG. A smooth particle-mesh-ewald method. J Chem Phys 1995;103:8577–8593.
58. Lennartz C, Schaefer A, Terstegen F, Thiel W. Enzymatic reactions of triosephosphate isomerase: a theoretical calibration study. J Phys Chem B 2002;106:1758–1767.
59. Siegbahn PEM. Theoretical study of the substrate mechanism of ribonucleotide reductase. J Am Chem Soc 1998;120:8417–8429.
60. Melo A, Ramos MJ, Floriano WB, Gomes JANF, Leão JFR, Magalhães AL, Maigret B, Nascimento MC, Reuter N. Theoretical study of arginine-carboxylate interactions. J Mol Struct (Theochem) 1999;463:81–90.
61. Ryde U. Carboxylate binding modes in zinc proteins: a theoretical study. Biophys J 1999;77:2777–2787.
62. Fernandes PA, Ramos MJ. Theoretical studies on the mechanism of inhibition of ribonucleotide reductase by (*E*)-2′-fluoromethylene-2′-deoxycitidine-5′-diphosphate. J Am Chem Soc 2003;125:6311–6322.
63. Fernandes PA, Ramos MJ. Theoretical studies on the mode of inhibition of ribonucleotide reductase by 2′-substituted substrate analogues. Chem Eur J 2003;9:5916–5925.
64. Lucas MF, Fernandes PA, Eriksson LA, Ramos MJ. Pyruvate formate lyase: a new perspective. J Phys Chem B 2003;107: 5751–5757.
65. Pereira S, Fernandes PA, Ramos MJ. Theoretical study of ribonucleotide reductase mechanism-based inhibition by 2′-azido-2′-deoxyribonucleoside 5′-diphosphates. J Comput Chem 2004;25:227–237.
66. Lee C, Yang WT, Parr RG. Development of the Colle-Salvetti correlation-energy formula into a functional of the electron density. Phys Rev B: Condens Matter 1988;37:785–789.
67. Becke AD. Density-functional thermochemistry. III. The role of exact exchange. J Chem Phys 1993;98:5648–5652.
68. Ziegler T. Approximate density functional theory as a practical tool in molecular energetics and dynamics. Chem Rev 1991;91:651–667.
69. Bauschlicher CW. A comparison of the accuracy of different functionals. Chem Phys Lett 1995;246:40–44.
70. Holthausen MC, Mohr M, Koch W. The performance of density functional/Hartree-Fock hybrid methods: the bonding in cationic first-row transition metal methylene complexes. Chem Phys Lett 1995;240:245–252.
71. Ricca A, Bauschlicher CW. A comparison of density functional theory with ab initio approaches for systems involving first transition row metals. Theor Chim Acta 1995;92:123–131.
72. Frisch MJ, Trucks GW, Schlegel HB, Scuseria GE, Robb MA, Cheeseman JR, Montgomery JA, Vreven T, Kudin KN, Burant JC, Millam JM, Iyengar SS, Tomasi J, Barone V, Mennucci B, Cossi M, Scalmani G, Rega N, Petersson GA, Nakatsuji H, Hada M, Ehara M, Toyota K, Fukuda R, Hasegawa J, Ishida M, Nakajima T, Honda Y, Kitao O, Nakai H, Klene M, Li X, Knox JE, Hratchin HP, Cross JB, Adamo C, Jaramillo J, Gomperts R, Stratmann RE, Yazyev O, Austin AJ, Cammi R, Pomelli C, Ochterski JW, Ayala PY, Morokuma K, Voth GA, Salvador P, Dannenberg JJ, Zakrzewski VG, Dapprich S, Daniels AD, Strain MC, Farkas O, Malik DK, Rabuck AD, Raghavachari K, Foresman JB, Ortiz JV, Cui Q, Baboul AG, Clifford S, Cioslowski J, Stefanov BB, Liu G, Liashenko A, Piskorz P, Komaromi I, Martin RL, Fox DJ, Keith T, Al-Lahan A, Peng CY, Nanayakkara A, Challacombe M, Gill PMW, Johnson B, Chen W, Wong MW, Gonzalez C, Pople JA. Gaussian 03, Revision A. 1. Pittsburg, PA: Gaussian; 2003.
73. Dolg M, Wedig U, Stoll H, Preuss H. Energy-adjusted ab initio pseudopotentials for the first row transition elements. J Chem Phys 1987;86:866–872.
74. Andrae D, Haussermann U, Dolg M, Stoll H, Preuss H. Energy-adjusted ab initio pseudopotentials for the second and third row transition elements. Theor Chim Acta 1990;77:123–141.
75. Frenking G, Antes I, Bohme M, Dapprich S, Ehlers AW, Jonas V, Neubaus A, Otto M, Stegmann R, Veldkamp A, Vyboishchi-

kov SF. Pseudopotential calculations of transition metal compounds: scope and limitations. Rev Comput Chem 1996;8:63–144.
76. Cances E, Mennucci B, Tomasi J. A new integral equation formalism for the polarizable continuum model: theoretical background and applications to isotropic and anisotropic dielectrics. J Chem Phys 1997;107:3032–3041.
77. Mennucci B, Tomasi J. Continuum solvation models: a new approach to the problem of solutes's charge distribution and cavity boundaries. J Chem Phys 1997;106:5151–5158.
78. Cossi M, Barone V, Mennucci B, Tomasi J. Ab initio study of ionic solutions by a polarizable continuum dielectric model. Chem Phys Lett 1998;286:253–260.
79. Cossi M, Scalmani G, Rega N, Barone V. New developments in the polarizable continuum model for quantum mechanical and classical calculations on molecules in solution. J Chem Phys 2002;117:43–54.
80. Cossi M, Rega N, Scalmani G, Barone V. Energies, structures, and electronic properties of molecules in solution with the C-PCM solvation model. J Comput Chem 2003;24:669–681.
81. Blomberg MRA, Siegbahn PEM, Babcock GT. Modeling electron transfer in biochemistry: a quantum chemical study of charge separation in *Rhodobacter sphaeroides* and photosystem II. J Am Chem Soc 1998;120:8812–8824.
82. Siegbahn PEM, Eriksson LA, Himo F, Pavlov M. Hydrogen atom transfer in ribonucleotide reductase (RNR). J Phys Chem B 1998;102:10622–10629.
83. Fernandes PA, Eriksson LA, Ramos MJ. The reduction of ribonucleotides catalyzed by the enzyme ribonucleotide reductase. Theor Chem Acc 2002;108:352–364.
84. Fernandes PA, Ramos MJ. Theoretical insights into the mechanism for thiol/disulfide exchange. Chem Eur J 2004;10:257–266.
85. Dapprich S, Komaromi I, Byun KS, Morokuma K, Frisch MJ. A new ONIOM implementation in Gaussian98. I. The calculation of energies, gradients, vibrational frequencies and electric field derivatives J Mol Struct (Theochem) 1999;461:1–21.
86. Vreven T, Morokuma K. On the application of the IMOMO (integrated molecular orbital plus molecular orbital) method. J Comput Chem 2000;21:1419–1432.
87. Stewart JJP. Optimization of parameters for semiempirical methods, Part 1: method. J Comput Chem 1989;10:209–220.
88. Stewart JJP. Optimization of parameters for semiempirical methods, Part 2: applications. J Comput Chem 1989;10:221–264.
89. Stewart JJP. Optimization of parameters for semiempirical methods, Part 3: extension of PM3 to Be, Mg, Zn, Ga, Ge, As, Se, Cd, In, Sn, Sb, Te, Hg, Tl, Pb, and Bi. J Comput Chem 1991;12:320–341.
90. Long SB, Casey PJ, Beese LS. Cocrystal structure of protein farnesyltransferase complexed with a farnesyl diphosphate substrate. Biochemistry 1998;37:9612–9618.
91. Dunten P, Kammlott U, Crowther R, Weber D, Palermo R, Birktoft J. Protein farnesyltransferase: structure and implications for substrate binding. Biochemistry 1998;37:7907–7912.
92. Dolence JM, Rozema DB, Poulter CD. Yeast protein farnesyltransferase. Site-directed mutagenesis of conserved residues in the β-subunit. Biochemistry 1997;36:9246–9252.
93. Kral AM, Diehl RE, deSolms SJ, Williams TM, Kohl NE, Omer CA. Mutational analysis of conserved residues of the β-subunit of human farnesyl: protein transferase. J Biol Chem 1997;272:27319–27323.
94. Koblan KS, Culberson JC, deSolms SJ, Giuliani EA, Mosser SD, Omer CA, Pitzenberger SM, Bogusky MJ. NMR studies of novel inhibitors bound to farnesyl-protein transferase. Protein Sci 1995;4:681.
95. Goldstein JL, Brown MS, Stradley SJ, Reiss Y, Gierasch LM. Nonfarnesylated tetrapeptide inhibitors of protein farnesyltransferase. J Biol Chem 1991;266:15575–15578.
96. Stradley SJ, Rizo J, Gierasch LM. Conformation of a heptapeptide substrate bound to protein farnesyltransferase. Biochemistry 1993;32:12586–12590.
97. Brown MS, Goldstein JL, Paris KJ, Burnier JP, Marsters JC, Jr. Tetrapeptide inhibitors of protein farnesyltransferase: amino-terminal substitution in phenylalanine-containing tetrapeptides restores farnesylation. Proc Natl Acad Sci USA. 1992;89:8313–8316.
98. Pompliano DL, Schaber MD, Mosser SD, Omer CA, Shafer JA, Gibbs JB. Isoprenoid diphosphate utilization by recombinant human farnesyl: protein transferase: interactive binding between substrates and a preferred kinetic pathway. Biochemistry 1993;32:8341–8347.
99. Dolence JM, Cassidy PB, Mathis JR, Poulter CD. Yeast protein farnesyltransferase: steady-state kinetic studies of substrate binding. Biochemistry 1995;34:16687–16694.
100. Yokoyama K, McGeady P, Gelb MH. Mammalian protein geranylgeranyltransferase. I. substrate specificity, kinetic mechanism, metal requirements, and affinity labeling. Biochemistry 1995;34:1344–1354.
101. Morokuma K, Musaev DG, Vreven T, Basch H, Torrent M, Khoroshun DV. Model studies of the structures, reactivities, and reaction mechanisms of metalloenzymes. IBM J Res Dev 2001;45:367–395.
102. Pelmenschikov V, Siegbahn PE. Catalytic mechanism of matrix metalloproteinases: two-layered ONIOM study. Inorg Chem 2002;41:5659–5666.
103. Torrent M, Vreven T, Musaev DG, Morokuma K, Farkas O, Schlegel HB. Effects of the protein environment on the structure and energetics of active sites of metalloenzymes. ONIOM study of methane monooxygenase and ribonucleotide reductase. J Am Chem Soc 2002;124:192–193.
104. Kuno M, Hannongbua S, Morokuma K. Theoretical investigation on nevirapine and HIV-1 reverse transcriptase binding site interaction, based on ONIOM method. Chem Phys Lett 2003;380:456–463.